I&EC research
Industrial & Engineering Chemistry Research

pubs.acs.org/IECR
Article

Using Molecular Conformers in COSMO-RS to Predict Drug Solubility in Mixed Solvents

Isabella W. Cordova, Gabriel Teixeira, Paulo J. A. Ribeiro-Claro, Dinis O. Abranches, Simão P. Pinho,* Olga Ferreira, and João A. P. Coutinho*

Cite This: *Ind. Eng. Chem. Res.* 2024, 63, 9565−9575

Read Online

ACCESS | Metrics & More | Article Recommendations | Supporting Information

ABSTRACT: This work explores the impact of solute conformers on the conductor-like screening model for real solvents (COSMO-RS) solubility predictions of vanillin and ethyl vanillin in water, short alcohols, and their mixed solvents. Two major conformers of these solutes and changes with solvent polarity were experimentally established by Raman spectroscopy and further confirmed by density functional theory calculations. The COSMO-RS predictions using the individual conformers show a poor description of the solubilities. Estimation with the COSMO-RS default conformer distribution gave better predictions and an intermediate behavior between the predictions obtained using each individual conformer. To further improve the description of the solubilities, the weight of each conformer was fitted to the experimental solid−liquid equilibrium data of the solute in a pure solvent at different temperatures. Better solubility predictions in ternary systems describing solubility maxima were found, suggesting a semipredictive approach to COSMO-RS. This method can predict the liquid−liquid oiling-out effect in the studied binary and ternary systems.

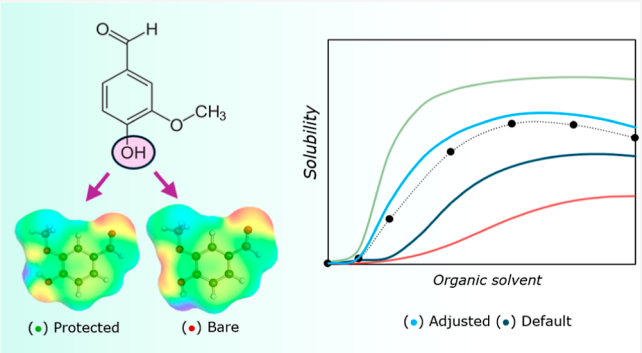

1. INTRODUCTION

Understanding and modeling phase equilibria is an essential step in the design of chemical processes. For example, solid−liquid equilibrium (SLE) data is crucial in the design of extractive crystallization,[1] which is widely applied to isolate and purify compounds in the pharmaceutical, chemical, and food industries.[2] Liquid−liquid equilibrium (LLE) can also play a role during an attempted crystallization through oiling-out or other immiscible liquid−liquid phenomena, which is often undesirable and can prevent the nucleation of the target solute.[2,3] On the other hand, the formation of a second liquid phase shifts the distribution of the compounds in the system, which can contribute to a decrease in the impurity content of the solid phase.[4,5] Nonetheless, understanding how temperature, the structure of the solute, and molecular-level mechanisms influence liquid−liquid phase separation remains limited.[6]

The correct description of LLE and SLE is also relevant to optimize purification processes through liquid−liquid extraction.[7−9] Aqueous solutions can be used as vehicles for carrying active pharmaceutical ingredients (APIs), although this might not be feasible for some compounds due to their low solubility, requiring high volumes of solvent for dissolution.[10] Besides, new drugs and drug-like compounds developed by high-throughput screening methods often present poor aqueous solubility, hindering their bioavailability.[11] One potential approach to overcome this solubility problem is to incorporate water-compatible cosolvents that can enhance the solubility of the target compound in the aqueous phase.[8−10] In addition to experimental measurements, often based on trial-and-error approaches, different solvent alternatives can be found by applying empirical and semiempirical models. The Jouyban−Acree model is one of the most used model to describe the solubility curves of APIs in mixed solvents, as highlighted by several studies.[10,12−16] Notably, the semipredictive two-liquid segment activity coefficient (NRTL-SAC) model proposed by Chen and Song[17,18] shows satisfactory results in the prediction of drug solubility.[18−20]

The fully predictive conductor-like screening model for real solvents (COSMO-RS) model,[21,22] based on quantum chemistry and statistical thermodynamics, can describe liquid−liquid and solid−liquid phase equilibria and has been successfully applied to predict aqueous solubilities of drugs[23] and solubility curves in mixtures of water and organic solvents.[24,25] However, challenges are still to be solved

Received: February 18, 2024
Revised: April 22, 2024
Accepted: April 30, 2024
Published: May 17, 2024

https://doi.org/10.1021/acs.iecr.4c00652
Ind. Eng. Chem. Res. 2024, 63, 9565−9575

concerning the prediction of poor aqueous drug solubility, with few approaches allowing for satisfactory results. In mixed solvents, the behavior of the solubility curves predicted with COSMO-RS differs drastically depending on the solute and solvent system, which may be a result of the molecular conformations (often just a single one) chosen to describe the solute. For example, Loschen and Klamt evaluated the solubility data of sulfadiazine, salicylic acid, prednisolone, and paracetamol in several solvent mixtures.[11] For systems with a maximum in the solubility curve, the qualitative description of the curve is reasonably consistent, although the location of the maxima is not well described. Other works indicate the inability of the model to predict solubility curves in a quantitative manner, emphasizing the inaccuracies that prevent its use in the selection of solvent mixtures for solubility enhancements.[26,27] Other variations of the COSMO model, such as COSMO-SAC (COSMO segment activity coefficient), were also tested to predict solubility in mixed solvents, with no consistent results.[28,29]

In this work, COSMO-RS was used to calculate the solubility of vanillin (VA) and ethyl vanillin (EVA) in water, short-chain alcohols, and their mixed solvents. The main objective was to predict both solid−liquid and liquid−liquid phase equilibria, focusing on the impact of solute conformations and intermolecular interactions of these very complex systems. This is the reason behind the choice of VA and EVA as model solutes as they both present complex phase equilibria in binary solvent mixtures at easily achievable temperatures. Furthermore, EVA is widely used as an additive in the food, perfume, and commodity industries.[30] VA is naturally found in vanilla beans and is the most widely used flavoring ingredient worldwide.[31] Due to the high cost of extraction, commercially available VA is mainly synthesized from the degradation of lignin.[31] In the purification of VA, the compound is capable of crystallizing into more than one polymorph, which highlights the importance of the correct description of phase equilibria.[2,32] In addition to their organoleptic properties, VA and its derivatives present antioxidant and anti-inflammatory activity.[33,34] Although the solubilities of VA and EVA in pure and mixed solvents were measured in several works,[5,6,32,35−40] only a few studies reported liquid−liquid phase separation in ternary mixtures of VA and EVA in short-chain alcohols and water.[5,6,35,41,42]

2. METHODOLOGY

2.1. Phase Equilibria Thermodynamics. After a series of common assumptions, the solubility of a solute, S, in a liquid solvent is described by the following SLE equation[43]

$$\ln(x_S\gamma_S) = \frac{\Delta_m h}{R}\left(\frac{1}{T_m} - \frac{1}{T}\right) + \frac{\Delta_m C_P}{R}\left(\frac{T_m}{T} - \ln\frac{T_m}{T} - 1\right) \tag{1}$$

where x_S is the mole fraction solubility of the solute in the system, γ_S is its activity coefficient, T_m and $\Delta_m h$ are its melting temperature and enthalpy, respectively, $\Delta_m C_P$ is its heat capacity change upon melting, R is the ideal gas constant, and T is the absolute temperature of the system. Given the small contribution of the heat capacity change term relative to that of the melting enthalpy term and recognizing that $\Delta_m C_P$ is typically not easily measurable or available in the literature, eq 1 can be further simplified to[43]

$$\ln(x_S\gamma_S) = \frac{\Delta_m h}{R}\left(\frac{1}{T_m} - \frac{1}{T}\right) \tag{2}$$

The melting temperature and enthalpy of VA ($\Delta_m h$ = 22.4 ±0.2 kJ/mol and T_m = 355.4 ± 0.1 K,[44]) and EVA ($\Delta_m h$ = 23.75 ±0.46 kJ/mol and T_m = 352.98 ± 0.50 K,[30]) were used in eq 2 for all solid−liquid phase equilibria calculations in this work.

Concerning liquid−liquid equilibria, the distribution of compound i between two liquid phases α and β is described by[43]

$$(x_i\gamma_i)^\alpha = (x_i\gamma_i)^\beta \tag{3}$$

2.2. COSMO-RS Model. COSMO-RS is a quantum chemistry and statistical thermodynamic-based model that predicts the activity coefficient (γ in eqs 1−3) of a compound in a mixture using a tessellated surface around a molecule embedded in a perfect dielectric continuum. This surface, known as the σ-surface (sigma surface), describes the screened charge densities of each tessellated surface segment of the molecule, from which COSMO-RS predicts excess Gibbs energies (and, thus, activity coefficients) through pairwise interactions between surface segments. In this work, all phase-equilibria-related calculations, including the implementation of COSMO-RS as well as the algorithms to solve eqs 1−3, were performed using the software package COSMOtherm[45] with the BP_TZVPD_FINE_21 parameterization.

Changing the geometry (i.e., conformer) chosen for any given molecule alters its sigma surface and, thus, the COSMO-RS-predicted activity coefficient. In this work, and as further explained in Section 3.1, two conformers of VA and EVA were optimized in the software package TURBOMOLE[46] through its COSMOBP-TZVPD-FINE template, which employs density functional theory (DFT) with the BP-86 functional, the triple-ζ valence polarized basis set with diffuse functions (def2-TZVPD), and a tessellation procedure yielding a fine grid. This DFT level of theory was chosen to be compatible with the aforementioned parameterization of COSMOtherm.

COSMO-RS is able to compute activity coefficients using different molecular conformers simultaneously. To do so, the population of the conformer j of a molecule with several conformers in a solvent S is weighted based on its free energy ($E_j^{COSMO} + \mu_j^S$) through a Boltzmann distribution[47]

$$\pi_j^S = \frac{w_j\, e^{\left\{\frac{E_j^{COSMO} + \mu_j^S}{kT}\right\}}}{\sum_{w_m} e^{\left\{\frac{E_m^{COSMO} + \mu_m^S}{kT}\right\}}} \tag{4}$$

where π_j^S is the fraction of all molecules found as conformer j and w_j is a weight prefactor that accounts for its state degeneracy (or multiplicity).

2.3. Quantum Mechanical Calculations. In addition to COSMO-RS, DFT calculations were also carried out for single molecules and small clusters using the Gaussian 09 software[48] using the built-in B3LYP functional with the 6-311+G(d,p) basis set. Geometry optimizations and frequency calculations were performed using the standard methods in Gaussian 09. Geometry optimizations were performed using the gradient method, and the final gradient length was less than 1×10^{-4} hartree Bohr^{-1} or hartree rad^{-1}, yielding geometries accurate to 0.05 pm or 0.1 Å. Frequency calculations were performed

https://doi.org/10.1021/acs.iecr.4c00652
Ind. Eng. Chem. Res. 2024, 63, 9565−9575

using analytical derivatives within the harmonic approximation. All the optimized structures were found to be real minima, with no imaginary frequencies. For calculated Raman and infrared spectra, vibrational frequencies were scaled by a factor of 0.967.[49] The Raman intensities were obtained from the calculated Raman activities, considering T = 298 K and ν_0 = 9200 cm^{-1}.

2.4. Raman Spectroscopy. Room-temperature Fourier transform Raman (FT-Raman) spectra of pure solvents and saturated solutions were recorded on a Bruker MultiRam FT-Raman spectrometer using an Nd:YAG laser with an excitation wavelength of 1064 nm and 2 cm^{-1} resolution. The final solvent and solution spectra are the average of 3 and up to 50 repeated measurements of 200 scans each, respectively.

3. RESULTS AND DISCUSSION

3.1. Conformer Analysis. Two conformers, hereby denoted as "protected" or "bare", were generated in this work for VA and for EVA. Their geometries, sigma surfaces, and sigma profiles (unnormalized histograms of sigma surfaces) are depicted in Figure 1. The "protected" conformers were obtained by rotating the hydroxyl group toward its methoxy or ethoxy counterpart, establishing an intramolecular hydrogen bond. On the other hand, "bare" conformers were generated aiming to maximize the intermolecular hydrogen bonding ability of the molecules by rotating the hydroxyl group in the opposite direction. These sets of conformers ("protected" and "bare") were chosen to represent the two polarity extremes of the ensemble of all possible molecular conformations for each compound.

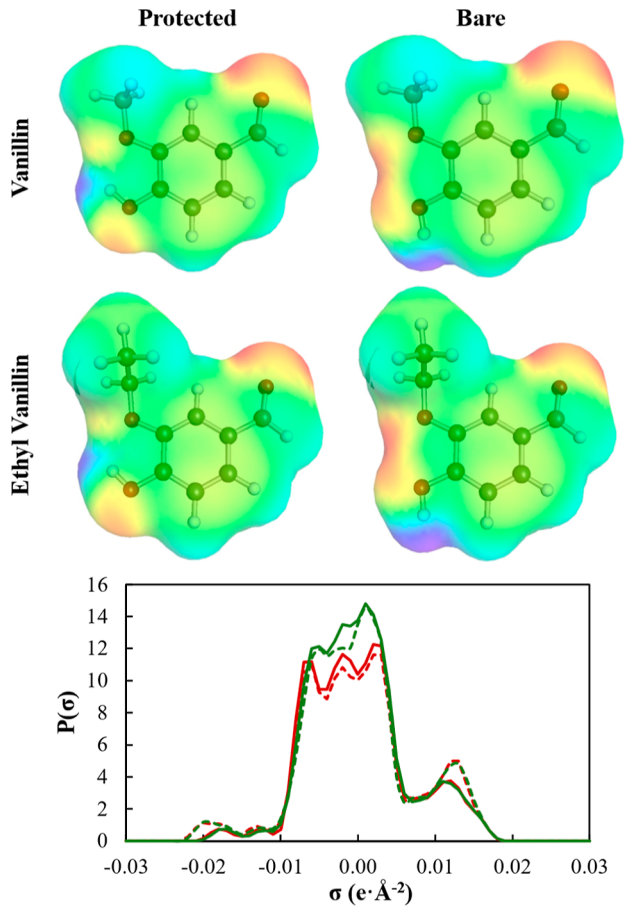

Figure 1. Optimized geometry and sigma surface of the protected and bare conformers of VA and EVA, as well as their corresponding sigma profiles (red and green lines represent VA and EVA, respectively, while full and dashed lines represent protected and bare conformers, respectively).

The sigma profiles depicted in Figure 1 show that all conformers present the highest peaks in the apolar region ($-0.01 < \sigma < 0.01$), representing the aromatic rings and alkyl substituents of both solutes. The sigma profile of EVA presents a higher apolar peak than that of VA due to the presence of an additional CH_2 group in the molecule. Moreover, while both molecules show the same sigma profile values in the hydrogen bond donor ($\sigma < -0.01$) and acceptor ($\sigma > -0.01$) regions due to having the same number of polar moieties, these values are larger for the bare conformers, corresponding to the exposure of additional molecular surfaces from the proton and oxygen. These surfaces are not available in the protected conformers due to intramolecular hydrogen bonding. As such, the bare conformer is expected to be prevalent in polar protic solvents such as water, where the solute maximizes its intermolecular hydrogen bonding capability to interact with the solvent, and the protected conformer is expected to be prevalent in apolar solvents.

The prevalence of the bare and protected conformers of VA in both water and ethanol was assessed through the self-consistent reaction field, which simulates the presence of a continuum polarized solvent medium around the solute, and the cluster method by adding solvent molecules to one solute molecule. Table 1 presents the relative energies of the two VA conformers (protected and bare) as isolated molecules, isolated molecules in a continuum solvent, and in cluster associations with up to three solvent molecules. Figure 2 shows the most stable cluster forms found for VA with three water molecules and with three ethanol molecules. These four-molecule clusters adopt the structure derived from the well-known square form of the $(H_2O)_4$ cluster.[50]

Table 1. Relative Energies (kJ mol^{-1}) of Protected/Bare Conformers of VA for the Single Molecule and for VA + Solvent Clusters Calculated at the B3LYP/6-311+G(d,p) Level of Theory

solvent	water		ethanol	
solute conformation	protected	bare	protected	bare
VA (single molecule)	0.0	21.2	0.0	21.2
VA (single molecule) SCR	0.0	10.8	0.0	11.4
VA + 1solvent	0.0	9.8	0.0	9.5
VA + 2solvent	0.0	4.9	0.0	6.1
VA + 3solvent	1.7	0.0	0.0	0.7

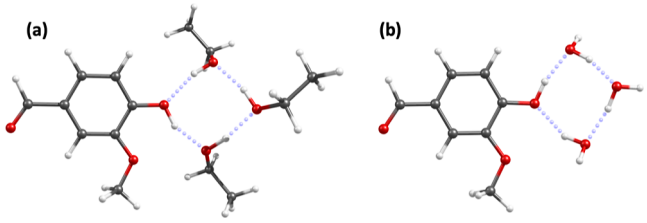

Figure 2. Optimized structures for VA−ethanol (a) and VA−water (b) clusters with one VA molecule and three solvent molecules at the B3LYP/6-311+G(d,p) level.

https://doi.org/10.1021/acs.iecr.4c00652
Ind. Eng. Chem. Res. 2024, 63, 9565−9575

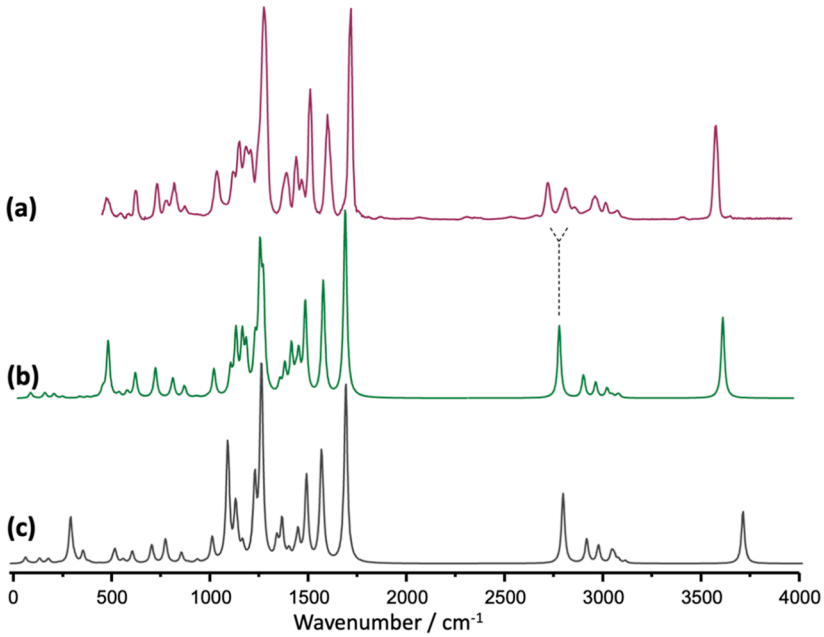

Figure 3. Experimental infrared spectrum for VA in the gas phase (a), as well as calculated infrared spectra for VA protected (b) and bare (c) conformers (single molecule).

As expected, the isolated molecule prefers the protected conformation, with a large energy difference relative to the bare conformation (ca. 21.2 kJ mol^{-1}). However, the most relevant result of Table 1 is the strong effect of the solvent on the relative energies of the protected/bare conformers. Both the continuum solvent model (SCR) and the direct interaction with one solvent molecule reduce the energy difference to nearly half. In the case of the clusters with three solvent molecules, the ethanol solvent reduces the bare-protected energy gap to ca. 0.7 kJ mol^{-1}, while water solvent inverts their stability ordering by ca. 1.7 kJ mol^{-1}. These structures (VA + 3solvent, illustrated in Figure 2) are only "snapshots" of possible structures in the liquid phase organization and cannot be considered representative of the diluted solution per se. However, they are indicative of a clear trend: the relative population of the two VA conformers in solution is affected by the solvent, and the effect of water is more pronounced than the effect of ethanol. Considering the energy differences in Table 1 for the VA + 3solvent clusters, the protected/bare conformer population is ca. 58%/42% in ethanol and ca. 32%/68% in water. All the above suggests that relying on single solute conformers to describe the solubility of VA in solvents through COSMO-RS does not properly capture the ensemble of solute−solvent interactions present in the mixture.

DFT calculations can be used to predict and interpret vibrational spectra, which in turn serve as a validation of the theoretical model. This "computational spectroscopy" approach has been successfully applied in recent studies by our group to diverse molecular systems, including eutectic mixtures,[51] biobased polymers,[52] and liquid alkoxysilane derivatives.[53] As such, the soundness of the present DFT calculations for VA is illustrated in Figure 3 by comparing the gas phase experimental infrared spectrum of VA, retrieved from the NIST database,[54] with the calculated spectra for the single VA molecule in protected and bare conformations. There is excellent agreement between the experimental and calculated spectra when considering the protected conformer (Figure 3, top and middle lines). The largest difference is observed for the stretching mode of the aldehyde C−H bond, for which the experimentally observed Fermi resonance splitting cannot be predicted from the harmonic approximation. In what concerns the bare conformer, there are significant differences relative to the experimental spectrum, namely, in the region of ca. 1000−1250 cm^{-1}, which will be further explored below. The comparison clearly validates the computational model herein used and supports the protected form as the dominant conformer in the gas phase.

As observed in Figure 3, the main differences between the infrared spectra of protected and bare conformers predicted from calculations arise in the 1000−1250 cm^{-1} range, a region where the vibrational modes associated with the phenolic COH group (namely, νC−O stretching and βC−O−H bending modes) are reported to occur.[50,55] The same behavior is observed for the Raman spectra when considering either the isolated molecule or the different clusters with water or ethanol (see Figure S1 of Supporting Information). In this way, this region is the most likely region for searching for the conformational equilibria of VA in the solution. Other regions showing small differences are generally difficult to isolate from the solvent, e.g., the νO−H stretching modes, for which the large band broadening cumulates with solvent bands overlap. Figure 4 presents the Raman spectra of VA solutions in carbon tetrachloride, ethanol, and water for the 1150−1550 cm^{-1} region after subtraction of the corresponding solvent spectrum.

Figure 4 clearly shows the effect of solvation in the Raman spectrum of VA. There are several changes observed in going from the nonpolar carbon tetrachloride solvent (ε = 2.3) to ethanol (ε = 24.3) and water (ε = 78.5), namely, in the band at ca. 1208 cm^{-1} (assigned to methyl rocking modes) and in the pair of bands at 1380 and 1402 cm^{-1} (ascribed to symmetric and asymmetric combinations of aldehydic C−H and phenolic O−H bending modes). However, the most relevant change occurs in the strong Raman band observed at ca. 1270 cm^{-1} in the carbon tetrachloride solution. This band correlates with the band observed at 1278 cm^{-1} in the crystalline form and assigned to the νC−O(H) stretching vibration, with

https://doi.org/10.1021/acs.iecr.4c00652
Ind. Eng. Chem. Res. 2024, 63, 9565−9575

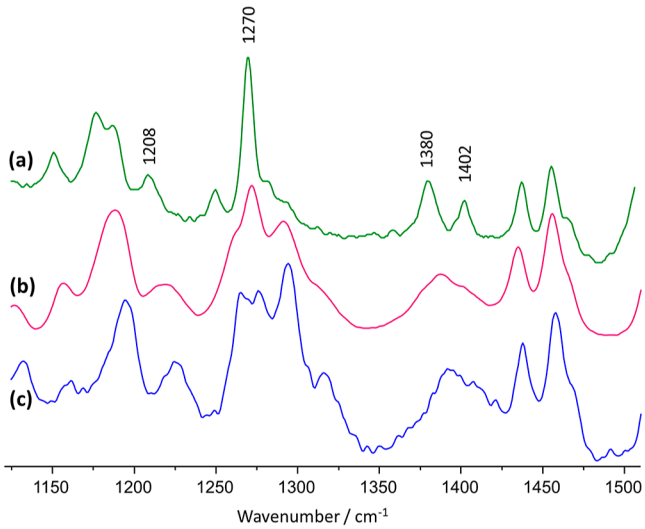

Figure 4. Difference Raman spectra (solution minus pure solvent) of VA solutions in carbon tetrachloride, ethanol, and water in the 1150−1550 cm^{-1} region. It is recognized that the procedure of subtracting solvent spectra can introduce artifacts, namely, due to solvent-induced band shifts and differences in band broadening. Subtraction spectra are used in this figure for the sake of clarity, and the nonsubtracted solution and solvent spectra are shown in Figure S2.

contribution from the βC−O−H bending mode.[50,55] In the crystalline structure of VA, only the protected conformer is present,[56] the same form that dominates the gas phase, as discussed above. In this way, the preference for the protected conformer is expected to hold for diluted VA in carbon tetrachloride, and the band at 1270 cm^{-1} is assigned to the νC−O stretching mode of this conformer. Upon dilution in ethanol, a second component of the νC−O mode arises in the high wavenumber side at ca. 1295 cm^{-1}, which is thus ascribed to the bare conformer of VA. Dilution in water originates a more complex band profile, but it is clear that it further intensifies the high wavenumber component associated with the bare conformer.

3.2. Standard COSMO-RS. The previous section established the different conformers of VA and EVA (i.e., protected and bare) studied and provided an extensive computational and experimental study of how VA changes its most prevalent conformer depending on the polarity of its environment. Now, the impact of conformer choice on the performance of COSMO-RS in the prediction of solubility is assessed. To do so, COSMO-RS was used to predict the solubility of VA and EVA in ethanol + water mixtures, employing either single conformers or the standard conformer weighting procedure (see Section 2.2). These results are depicted in Figure 5, along with the corresponding experimental solubility curves.

There is a significant difference in the solubility predictions based on the solute conformation. As expected, by rotating the hydroxyl group of the solute outward, hydrogen bonding intermolecular interactions increased, and the model overestimated the solubility when only the bare conformer was considered (dotted lines in Figure 5). Likewise, by rotating the hydroxyl group inward, hydrogen bonding intermolecular interactions drastically diminished, underestimating the solubility values (dashed lines in Figure 5). When both conformers are used through the default conformer weighting method of COSMO-RS (eq 4 of Section 2.2), an intermediate solubility curve is obtained (dashed−dotted lines in Figure 5), representing a more satisfactory prediction when compared with the experimental data.

The behavior identified above, with protected and bare conformers systematically underestimating and overestimating solubility, respectively, is not exclusive to the water/ethanol mixed solvent. To show this, solubility predictions for VA and EVA in methanol + water and 1-propanol + water are depicted in Figure S3 of Supporting Information. These results are identical to those reported in Figure 5. Moreover, this COSMO-RS prediction pattern is also seen at other temperatures, as shown in Figure S4, showing solubility predictions for all three mixed solvents (water + methanol, ethanol, or 1-propanol) in a larger temperature range. Finally, it is relevant to note that despite the lack of quantitative agreement, both the individual conformers and the conformer set distribution qualitatively describe the solubility curves in all studied ternary systems.

The conformer distribution π_j^S obtained through the default conformer weighting method of COSMO-RS (eq 4 of Section 2.2) is reported in Figure 6 for the organic solvent + water solvent mixtures mentioned above. As expected, the concentration of the "bare" conformer is higher in the water-rich solvent mixtures, representing nearly 80% of the conformer ensemble of both VA and EVA in pure water. This is consistent with the fact that the "bare" conformer has the hydroxyl group prone to hydrogen bonding interactions and is close to the 68% value predicted by DFT calculations in Section 3.1 for VA.

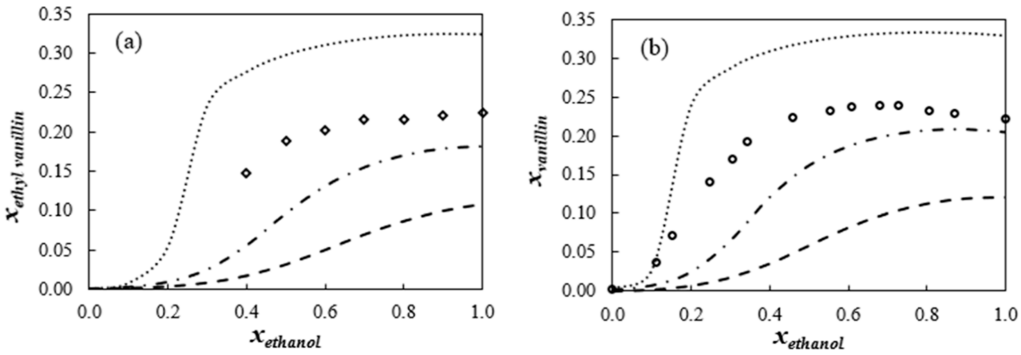

Figure 5. Predicted and experimental mole fraction solubilities of EVA (a) and VA (b) in ethanol + water mixtures at 303.15 K. The COSMO-RS predictions were calculated using the default conformer set distribution (dashed−dotted lines), "bare" conformer (dotted lines), and "protected" conformer (dashed lines). Symbols represent experimental data from literature: ◇ Guo et al.[37] and ○ Hamedi et al.[40]

https://doi.org/10.1021/acs.iecr.4c00652
Ind. Eng. Chem. Res. 2024, 63, 9565−9575

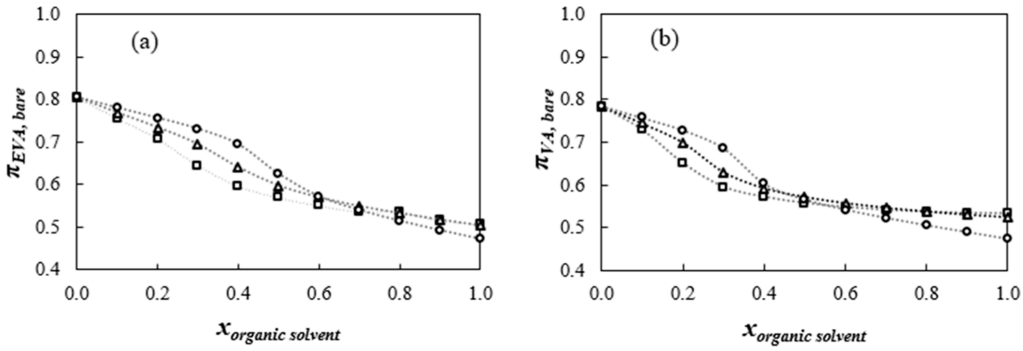

Figure 6. Distribution of the "bare" conformers of EVA (a) and VA (b) in organic solvent + water mixtures at 313.15 K using the conformer set default distribution of COSMO-RS. Symbols represent different solvent systems: □ 1-propanol + water, Δ ethanol + water, and ○ methanol + water.

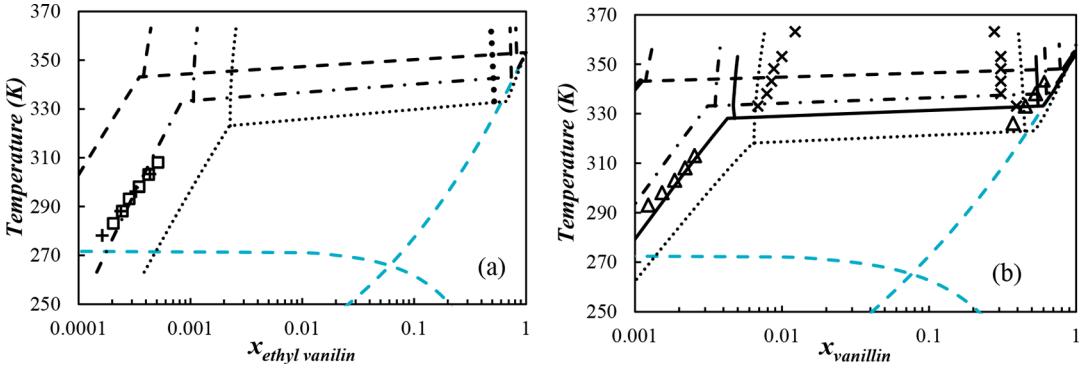

Figure 7. Predicted and experimental mole fraction solubilities of EVA (a) and VA (b) in water at several temperatures. The COSMO-RS predictions were calculated using the default conformer set distribution (dashed−dotted lines), adjusted conformer weight (solid lines), "bare" conformer (dotted lines), and "protected" conformer (dashed lines). Blue dashed lines represent the ideal behavior of the mixture. Symbols represent experimental data taken from literature: □ Zhang et al. (2022),[6] + Hussain et al. (2001),[32] × Svärd et al. (2007),[41] and Δ Cesari et al. (2017).[57]

Figure 6 also shows that the COSMO-RS-predicted prevalence of "bare" conformers decreases with increasing alcohol concentration, reaching approximately 50% in pure alcohol, close to the DFT predicted value of 42%. Interestingly, there is a changing point in the conformer distribution approximately at $x_{solvant}$ = 0.6 and $x_{solvant}$ = 0.4 of EVA and VA, respectively. In fact, over these concentrations, the conformer distribution in the different systems remains very similar and quite constant, showing some similarity to the solubility curves at higher organic solvent concentrations, where solubility does not change much. Additionally, before reaching the changing point mole fraction, the "bare" conformer presents a higher distribution frequency in the methanol + water system compared to that of the other systems, while above is the opposite. The changing points of the conformer distribution may indicate a shift in the solubilization mechanism.

3.3. Custom Conformer Weighting. The poor COSMO-RS quantitative description of solubility reported above, even when both bare and protected conformers are used simultaneously, combined with the discrepancy between COSMO-RS and DFT-predicted conformer distributions, suggests that the default conformer weighting method of COSMO-RS (eq 4 of Section 2.2) may not be the best approach to describe the conformer distribution of VA and EVA in the studied systems. Note that COSMO-RS already fails to quantitatively predict the solubility of these solutes in the pure alcohols studied, an inaccuracy that is carried over to the mixed solvent predictions. As such, a semiempirical treatment of conformers is developed and tested in this section.

Rather than taking conformer prefactors (w_j) in eq 4 to be constant values related to state degeneracies, these can be exploited as concentration-dependent empirical fitting parameters. To do so, a simple linear mixing rule for these prefactors was defined as

$$w_{j,\text{mixture}} = (w_{j,\text{solute+organic solvent}} - w_{j,\text{solute+water}}) \cdot x_{\text{organic solvent}} + w_{j,\text{solute+water}} \quad (5)$$

where $w_{j,\text{solute+organic solvent}}$ and $w_{j,\text{solute+water}}$ are the fitting parameters of conformer j in solute/alcohol and solute/water mixtures, respectively, $x_{\text{organic solvent}}$ is the alcohol mole fraction in the binary mixture solvent (water + alcohol), and $w_{j,\text{mixture}}$ is the fitting parameter of conformer j in the ternary solute/alcohol/water mixture. Furthermore, note that w_j is being constrained to the range from 0 to 1, with $w_{j=\text{bare}} = 1 - w_{j=\text{protected}}$. Thus, and considering eq 4, the boundary values of this range represent single conformers.

The prefactors of eq 5 were fitted to experimental SLE data of binary mixtures of the solute (VA or EVA) in a pure solvent (water or alcohol), measured at different temperatures. This fitting, reported in Figures S5 and S6 of Supporting Information, was carried out considering the conformer weight that presented the best representation of the SLE phase diagram in comparison to the experimental data based on the minimization of the root-mean-square deviation (rmsd)

https://doi.org/10.1021/acs.iecr.4c00652
Ind. Eng. Chem. Res. 2024, 63, 9565−9575

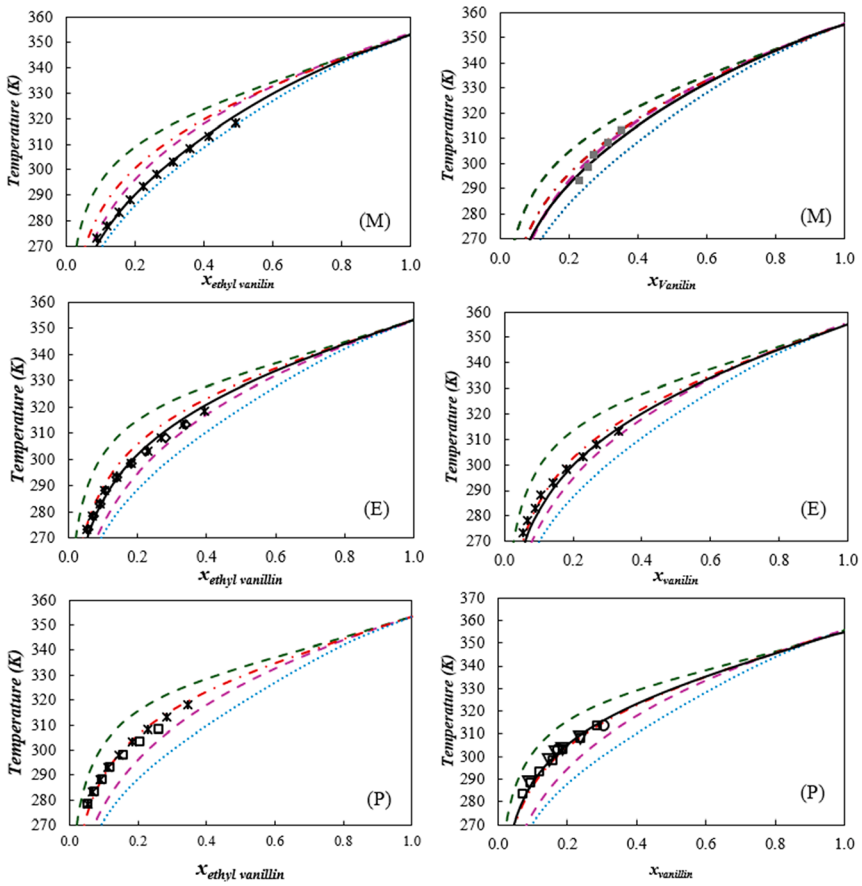

Figure 8. Predicted and experimental mole fraction solubilities of EVA (left) and VA (right) in methanol (M), ethanol (E), and 1-propanol (P) at several temperatures. The COSMO-RS predictions were calculated using the default conformer set distribution (red dashed-dotted lines), adjusted conformer prefactor (solid lines), "bare" conformer (blue dotted lines) and "protected" conformer (green dashed lines). Purple dashed lines represent the ideal behavior of the mixture. Symbols represent experimental data taken from literature: □ ref 6, + ref 30, ▽ ref 35, ○ ref 40, ▽ ref 35, and ■ obtained in this work (see Table S1).

$$\text{rmsd} = \sqrt{\frac{\sum_{i=1}^{N} (T_{\text{calc}} - T_{\text{exp}})^2}{N}} \tag{6}$$

where T_{calc} is the calculated equilibrium temperature for a given set of conformer weights at a fixed solute mole fraction composition, T_{exp} is the corresponding experimental value, and N is the number of experimental points.

Conformer fitting parameters were obtained for EVA and VA in water using SLE data, as reported in Figures S5 and S6, yielding $w_{j=\text{bare}} = 0.50$ and $w_{j=\text{bare}} = 0.62$, respectively. Note that a value of 0.50 leads to $w_{j=\text{bare}} = w_{j=\text{protected}}$. Thus, because COSMO-RS considers the same degeneracy for all studied conformers, a prefactor value of 0.50 is identical to the default conformer weight method of COSMO-RS. The complete SLLE phase diagrams of VA/water and EVA/water are depicted in Figure 7, showing that (i) using both conformers simultaneously yields better results than using only either bare or protected conformers and (ii) there is little to no improvement when fitting the prefactors of eq 4 to experimental data, with the default values of COSMO-RS providing a remarkable description of the binary phase diagram, including the formation of a liquid−liquid separation for VA/water, in agreement with experimental data.

Much like the case for water, conformer fitting parameters were also obtained for VA and EVA in methanol, ethanol, or 1-propanol using SLE data, as reported in Figures S5 and S6. However, in contrast with the water-based binary mixtures, here the fitting of the empirical prefactors improves results in nearly all instances (Figure 8).

All in all, fitting the prefactors of eq 4 to experimental binary solute/solvent data improves the performance of COSMO-RS, as expected, with the average rmsd decreasing from 5.8 to 1.8. Of course, the quality of the experimental data is crucial for this approach; for systems with few experimental data points such as VA + methanol, more experimental data from different sources would be desirable.

The true advantage of the approach developed so far lies in the fact that the turned-fitting-parameter prefactors, which were fitted only to binary systems, can now be combined with the linear mixing rule of eq 5 to predict SLE in ternary mixtures. These results are reported in Figure 9 for the ternary mixtures previously assessed in Section 3.2.

The predictions with empirical prefactors (fitted using only the experimental solubility data in the pure solvents) show a much better description of the solubility curves in the mixed solvents. For all systems studied, the underprediction of the solubility curves obtained using the standard COSMO-RS approach (eq 4 without empirical prefactors) is greatly reduced. The root mean squared relative error (RMSRE) of the prediction in the ternary systems is reported in Table S2, highlighting the better results for 1-propanol + water + VA, ethanol + water + VA, and ethanol + water + EVA systems. For

https://doi.org/10.1021/acs.iecr.4c00652
Ind. Eng. Chem. Res. 2024, 63, 9565−9575

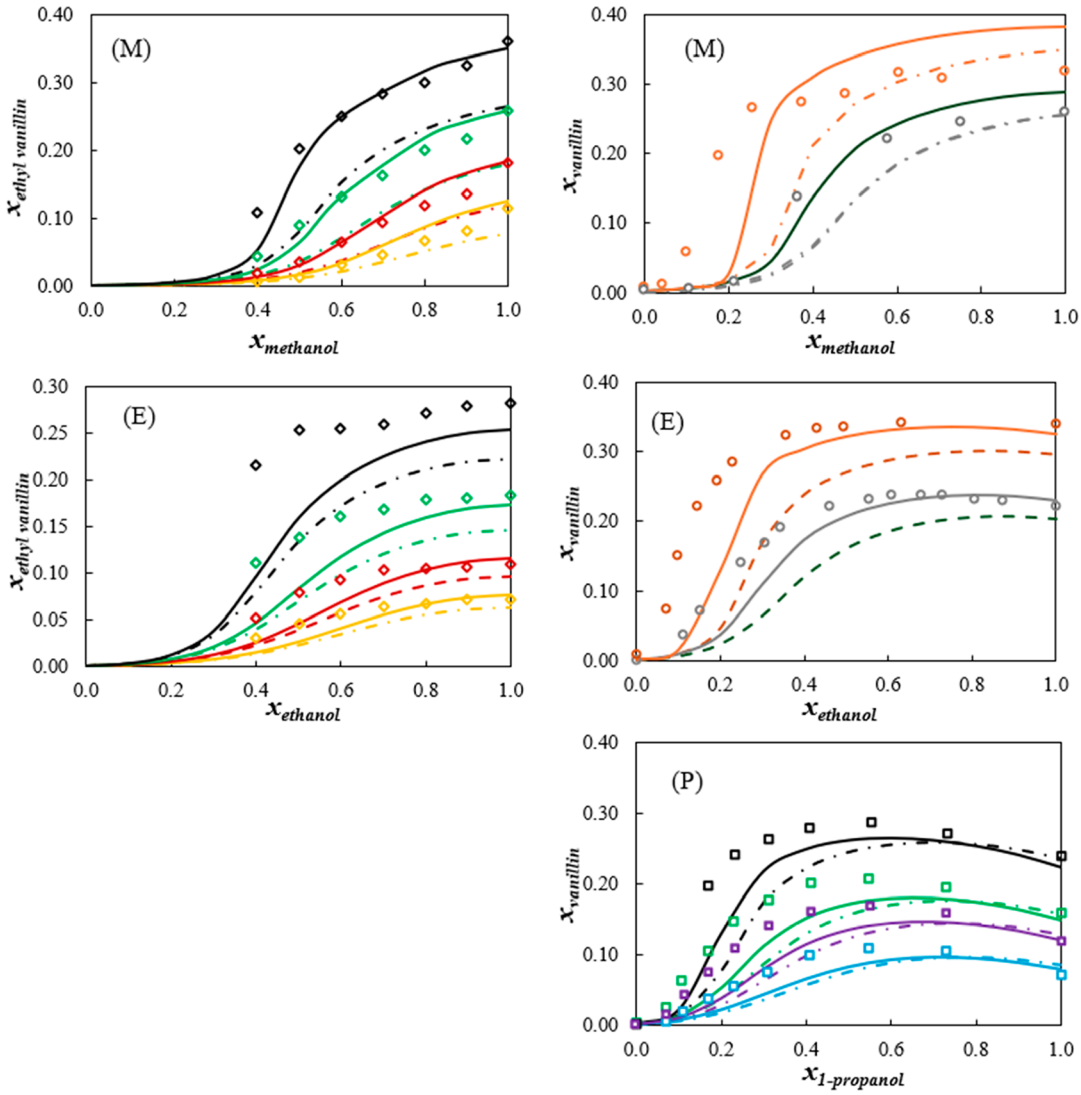

Figure 9. Predicted and experimental mole fraction solubilities of EVA (left) or VA (right) in methanol + water (M), ethanol + water (E), and 1-propanol + water (P) mixtures. The COSMO-RS predictions were calculated using the default conformer set distribution (dashed−dotted lines) and calculated conformer prefactor (solid lines). Different colors represent different temperatures: orange: 313.15, black: 308.15, gray: 303.15, green: 298.15, dark purple: 293.15, red: 288.15, light purple: 283.15, and yellow: 278.15 K. Symbols represent experimental data taken from literature: □ ref 6, ◇ ref 37, and ○ ref 40.

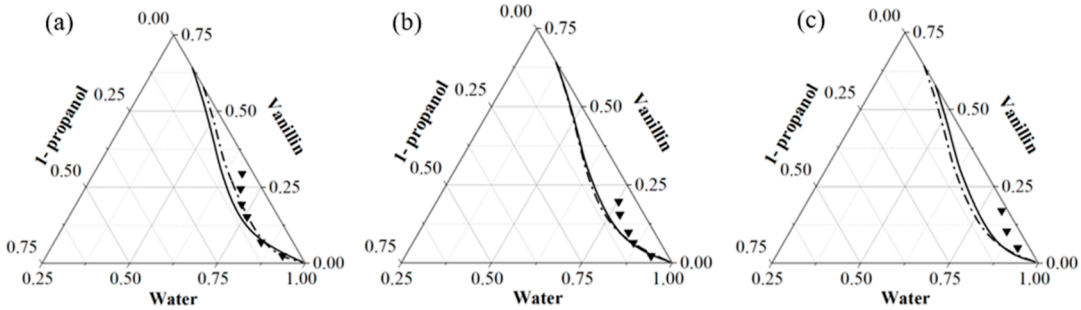

Figure 10. Predicted and experimental liquid−liquid equilibria of VA in 1-propanol + water mixtures at 303.15 (a), 308.15 (b), and 313.15 K (c) in molar fraction using the COSMOBP-TZVPD-FINE template. The COSMO-RS predictions were calculated using the default conformer set distribution (dashed−dotted lines) and calculated conformer weight (solid lines). Triangles represent experimental data taken from Du et al. (2016).[35]

the ternary systems with methanol, the composition of the solvent where the inflection in the solubility curve occurs is better estimated. However, the RMSRE indicates that the overall description of the solubility is better than the default distribution of conformers. For ethanol + water + EVA at 308.15 K, the predictions using both the default distribution

https://doi.org/10.1021/acs.iecr.4c00652
Ind. Eng. Chem. Res. 2024, 63, 9565−9575

and the fitted conformer prefactors are worse in comparison with the other temperatures in the same system. The new conformer distributions throughout the mixtures assessed using eq 5 combined with eq 4 are depicted in Figure S7.

3.4. Liquid−Liquid Equilibrium. The custom method developed in the previous section greatly expands the predictive capability of COSMO-RS at the expense of using binary data for fitting purposes. This predictive capability is now further tested by predicting ternary LLE phase diagrams using the fitted prefactors reported in the previous section, obtained using only binary SLE data. COSMO-RS predictions and SLE experimental data revealed a weak solute interaction in the water-rich solvents, particularly for VA, as indicated by the low solubility values. The poor intermolecular interactions between water and VA and its low melting point contribute to the formation of a second liquid phase. This is prone to the induction of an oiling-out of VA, which corresponds to the separation of VA into a second liquid phase when attempting to crystallize VA, as shown in Figure 10. This phenomenon can be observed at low concentrations of the alcohol.

The oiling-out effect observed in the ternary diagrams depicted in Figure 10 can be attributed to the hydrophobic nature of VA, with a liquid−liquid phase separation arising from the weak interaction between water and VA in the water-dominated region. Remarkably, COSMO-RS is able to predict the liquid−liquid separation (oiling-out) in the ternary system while consistently overestimating the liquid−liquid region, in particular the solubility of water in VA, and the predictions worsen with increasing temperature as the COSMO-RS predictions exhibit minimal temperature dependence for the LLE region.

Paduszyński and Królikowska (2020) predicted LLE phase diagrams in binary systems, analyzing the impact of the computational level (COSMOBP-TZVP and COSMOBP-TZVPD-FINE) on the accuracy of the calculations, with the COSMOBP-TZVP template presenting more accurate predictions when compared to those of COSMOBP-TZVPD-FINE.[58] The prediction of the oiling-out effect of VA at the TZVP level is shown in Figure S8. In fact, the liquid−liquid region is less overestimated at a less complex level of calculation, although the minimal temperature dependence of the predictions for the LLE region persists.

4. CONCLUSIONS

This study explores the influence of solute conformation on phase equilibria predictions by quantifying it using COSMO-RS and DFT calculations, as well as experimentally by using Raman spectroscopy. Through DFT calculations, we were able to explore the interactions of the solutes with solvent media regarding their conformation preferences, validating the use and impact of the proportion of each solute conformation in the COSMO-RS predictions, ultimately suggesting moving toward a better physical-chemistry description of the mixtures using a more realistic conformer distribution. Raman spectroscopy and DFT calculations confirmed the presence of two major conformers in VA, whose relative proportions depend on the solvent polarity. For VA and EVA, the hydroxyl group rotation strongly affects the ability of these compounds to establish hydrogen bonding interactions with the solvent media, and the most stable conformer in vacuum does not necessarily provide the best description of the phase behavior. Therefore, understanding and describing conformer distributions is essential to adequately capture in COSMO-RS the solute−solvent interactions that rule phase behavior.

The experimental data compiled in this work shows a cosolvency phenomenon between water and 1-propanol, ethanol, and methanol to improve the solubility of model solutes VA and EVA. EVA presents lower solubility values than those of VA, as correctly predicted by the COSMO-RS model. The COSMO-RS also successfully predicted the shape of the solubility curves for all studied systems, satisfactorily describing the cosolvency.

The default distribution of conformers provides a good description of all binary systems, including those presenting strong deviations from ideality. Using that distribution in the water + VA system, liquid−liquid phase separation is calculated, in agreement with the experimental data. In the ternary systems, the solubility curves show a good qualitative description, although the solubility maximum enhancement is not accurately described.

Fitting the conformer weight of the solutes provided better predictions than the default conformation for solid−liquid equilibria calculations, enhancing the description of the location and value of the solubility maxima. This COSMO-RS-based semipredictive approach proposed requires experimental values of the solubility of the target solute in pure solvents. However, it is effective as it improves the results concerning the solubility of mixed solvents and highlights the importance of the distribution of conformers throughout the solvent mixtures and its impact on solubility predictions.

Finally, despite the minimal temperature dependence, the COSMO-RS model effectively identifies and qualitatively describes the liquid−liquid region in the ternary systems. The oiling-out effect phenomenon hinders the solubilization solute crystallization of hydrophobic solutes, and consequently, predicting the oiling-out effect is also crucial in the design, control, and optimization of crystallization and purification processes.

■ ASSOCIATED CONTENT

Supporting Information

The Supporting Information is available free of charge at https://pubs.acs.org/doi/10.1021/acs.iecr.4c00652.

VA infrared spectra; predicted and experimental solubilities of the selected ternary systems; rmsd and fitting of the conformer prefactor; conformer distribution; predicted and experimental liquid−liquid equilibria of VA in binary mixtures; experimental solubility of VA in methanol obtained in this work; and RMSRE of the solubility predictions in ternary systems (PDF)

■ AUTHOR INFORMATION

Corresponding Authors

Simão P. Pinho − *Centro de Investigação de Montanha, Instituto Politécnico de Bragança, 5300-253 Bragança, Portugal; Laboratório para a Sustentabilidade e Tecnologia em Regiões de Montanha, Instituto Politécnico de Bragança, 5300-253 Bragança, Portugal;* orcid.org/0000-0002-9211-857X; Email: spinho@ipb.pt

João A. P. Coutinho − *CICECO, Aveiro Institute of Materials, Complexo de Laboratórios Tecnológicos, Aveiro University, 3810-193 Aveiro, Portugal;* orcid.org/0000-0002-3841-743X; Email: jcoutinho@ua.pt

https://doi.org/10.1021/acs.iecr.4c00652
Ind. Eng. Chem. Res. 2024, 63, 9565−9575

Authors

Isabella W. Cordova − *CICECO, Aveiro Institute of Materials, Complexo de Laboratórios Tecnológicos, Aveiro University, 3810-193 Aveiro, Portugal; Centro de Investigação de Montanha, Instituto Politécnico de Bragança, 5300-253 Bragança, Portugal; Laboratório para a Sustentabilidade e Tecnologia em Regiões de Montanha, Instituto Politécnico de Bragança, 5300-253 Bragança, Portugal*

Gabriel Teixeira − *CICECO, Aveiro Institute of Materials, Complexo de Laboratórios Tecnológicos, Aveiro University, 3810-193 Aveiro, Portugal;* orcid.org/0000-0002-5213-5359

Paulo J. A. Ribeiro-Claro − *CICECO, Aveiro Institute of Materials, Complexo de Laboratórios Tecnológicos, Aveiro University, 3810-193 Aveiro, Portugal;* orcid.org/0000-0001-5171-2153

Dinis O. Abranches − *CICECO, Aveiro Institute of Materials, Complexo de Laboratórios Tecnológicos, Aveiro University, 3810-193 Aveiro, Portugal;* orcid.org/0000-0003-0097-2072

Olga Ferreira − *Centro de Investigação de Montanha, Instituto Politécnico de Bragança, 5300-253 Bragança, Portugal; Laboratório para a Sustentabilidade e Tecnologia em Regiões de Montanha, Instituto Politécnico de Bragança, 5300-253 Bragança, Portugal;* orcid.org/0000-0001-8414-3479

Complete contact information is available at: https://pubs.acs.org/10.1021/acs.iecr.4c00652

Notes

The authors declare no competing financial interest.

■ ACKNOWLEDGMENTS

This work was developed within the scope of the project CICECO-Aveiro Institute of Materials, UIDB/50011/2020, UIDP/50011/2020, and LA/P/0006/2020, and CIMO-Mountain Research Center, UIDB/00690/2020 and LA/P/0007/2020, financed by national funds through the Portuguese Foundation for Science and Technology/MCTES. G.T. thanks FCT for his Ph.D. grant (UI/BD/151114/2021). I.W.C. thanks FCT for her Ph.D. grant (2022.12407.BD).

■ REFERENCES

(1) Ouyang, J.; Xing, X.; Chen, J.; Zhou, L.; Liu, Z.; Heng, J. Y. Y. Effects of Solvent, Supersaturation Ratio and Silica Template on Morphology and Polymorph Evolution of Vanillin during Swift Cooling Crystallization. *Particuology* **2022**, *65*, 93−104.

(2) Duffy, D.; Cremin, N.; Napier, M.; Robinson, S.; Barrett, M.; Hao, H.; Glennon, B. In Situ Monitoring, Control and Optimization of a Liquid-Liquid Phase Separation Crystallization. *Chem. Eng. Sci.* **2012**, *77*, 112−121.

(3) Lafferrère, L.; Hoff, C.; Veesler, S. In Situ Monitoring of the Impact of Liquid-Liquid Phase Separation on Drug Crystallization by Seeding. *Cryst. Growth Des.* **2004**, *4* (6), 1175−1180.

(4) Tanaka, K.; Takiyama, H. Effect of Oiling-Out during Crystallization on Purification of an Intermediate Compound. *Org. Process Res. Dev.* **2019**, *23* (9), 2001−2008.

(5) Zhao, H.; Xie, C.; Xu, Z.; Wang, Y.; Bian, L.; Chen, Z.; Hao, H. Solution Crystallization of Vanillin in the Presence of a Liquid-Liquid Phase Separation. *Ind. Eng. Chem. Res.* **2012**, *51* (45), 14646−14652.

(6) Zhang, H.; Zhang, K.; Yu, M.; Guo, J.; Xu, S.; Wang, Y. Insight into Solid-Liquid and Liquid-Liquid Phase Equilibrium Behavior of Vanillin and Ethyl Vanillin. *J. Mol. Liq.* **2022**, *365*, 120059.

(7) Mao, H.; Chen, H.; Jin, M.; Wang, C.; Xiao, Z.; Niu, Y. Measurement and correlation of solubility of o-vanillin in different pure and binary solvents at temperatures from 273.15 K to 303.15 K. *J. Chem. Thermodyn.* **2020**, *150*, 106199.

(8) Cárdenas, Z. J.; Almanza, O. A.; Jouyban, A.; Martínez, F.; Acree, W. E. Solubility and Preferential Solvation of Phenacetin in Methanol + Water Mixtures at 298.15 K. *Phys. Chem. Liq.* **2018**, *56* (1), 16−32.

(9) Li, W.; Lu, H. T.; Doblin, M. S.; Bacic, A.; Stevens, G. W.; Mumford, K. A. A Solvent Loss Study for the Application of Solvent Extraction Processes in the Pharmaceutical Industry. *Chem. Eng. Sci.* **2022**, *250*, 117400.

(10) Soltanpour, S.; Jouyban, A. Solubility of Acetaminophen and Ibuprofen in Polyethylene Glycol 600, N-Methyl Pyrrolidone and Water Mixtures. *J. Solution Chem.* **2011**, *40* (12), 2032−2045.

(11) Loschen, C.; Klamt, A. Solubility Prediction, Solvate and Cocrystal Screening as Tools for Rational Crystal Engineering. *J. Pharm. Pharmacol.* **2015**, *67* (6), 803−811.

(12) Abbasi, M.; Martinez, F.; Jouyban, A. Prediction of Deferiprone Solubility in Aqueous Mixtures of Ethylene Glycol, Propylene Glycol and Polyethylene Glycol 400 at Various Temperatures. *J. Mol. Liq.* **2014**, *197*, 171−175.

(13) Qiu, J.; Huang, H.; He, H.; Liu, H.; Hu, S.; Han, J.; Yi, D.; An, M.; Guo, Y.; Wang, P. Solubility Determination and Thermodynamic Modeling of Edaravone in Different Solvent Systems and the Solvent Effect in Pure Solvents. *J. Chem. Eng. Data* **2020**, *65* (6), 3240−3251.

(14) Dadmand, S.; Kamari, F.; Acree, W. E.; Jouyban, A. Solubility Prediction of Drugs in Binary Solvent Mixtures at Various Temperatures Using a Minimum Number of Experimental Data Points. *AAPS PharmSciTech* **2019**, *20* (1), 10.

(15) Rahimpour, E.; Alvani-Alamdari, S.; Acree, W. E.; Jouyban, A. Drug Solubility Correlation Using the Jouyban-Acree Model: Effects of Concentration Units and Error Criteria. *Molecules* **2022**, *27* (6), 1998.

(16) Jouyban, A.; Chan, H. K.; Chew, N. Y. K.; Khoubnasabjafari, M.; Acree Jr, W. E. Solubility Prediction of Paracetamol in Binary and Ternary Solvent Mixtures Using Jouyban-Acree Model. *Chem. Pharm. Bull.* **2006**, *54* (4), 428−431.

(17) Chen, C. C.; Song, Y. Solubility Modeling with a Nonrandom Two-Liquid Segment Activity Coefficient Model. *Ind. Eng. Chem. Res.* **2004**, *43* (26), 8354−8362.

(18) Chen, C. C.; Crafts, P. A. Correlation and Prediction of Drug Molecule Solubility in Mixed Solvent Systems with the Nonrandom Two-Liquid Segment Activity Coefficient (NRTL-SAC) Model. *Ind. Eng. Chem. Res.* **2006**, *45* (13), 4816−4824.

(19) Mota, F. L.; Queimada, A. J.; Andreatta, A. E.; Pinho, S. P.; Macedo, E. A. Calculation of Drug-like Molecules Solubility Using Predictive Activity Coefficient Models. *Fluid Phase Equilib.* **2012**, *322*−*323*, 48−55.

(20) Mirheydari, S. N.; Barzegar-Jalali, M.; Acree, W. E.; Shekaari, H.; Shayanfar, A.; Jouyban, A. Comparison of the Models for Correlation of Drug Solubility in Ethanol + Water Binary Mixtures. *J. Solution Chem.* **2019**, *48* (7), 1079−1104.

(21) Klamt, A. Conductor-like Screening Model for Real Solvents: A New Approach to the Quantitative Calculation of Solvation Phenomena. *J. Phys. Chem.* **1995**, *99* (7), 2224−2235.

(22) Klamt, A.; Eckert, F. COSMO-RS: A Novel and Efficient Method for the a Priori Prediction of Thermophysical Data of Liquids. *Fluid Phase Equilib.* **2000**, *172* (1), 43−72.

(23) Klamt, A.; Eckert, F.; Hornig, M.; Beck, M. E.; Burger, T. Prediction of Aqueous Solubility of Drugs and Pesticides with COSMO-RS. *J. Comput. Chem.* **2002**, *23* (2), 275−281.

(24) Tang, W.; Wang, Z.; Feng, Y.; Xie, C.; Wang, J.; Yang, C.; Gong, J. Experimental Determination and Computational Prediction of Androstenedione Solubility in Alcohol + Water Mixtures. *Ind. Eng. Chem. Res.* **2014**, *53* (28), 11538−11549.

(25) Abranches, D. O.; Benfica, J.; Shimizu, S.; Coutinho, J. A. P. Solubility Enhancement of Hydrophobic Substances in Water/Cyrene Mixtures: A Computational Study. *Ind. Eng. Chem. Res.* **2020**, *59* (40), 18247−18253.

(26) Cysewski, P.; Jeliński, T.; Cymerman, P.; Przybylek, M. Solvent Screening for Solubility Enhancement of Theophylline in Neat, Binary and Ternary NADES Solvents: New Measurements and Ensemble Machine Learning. *Int. J. Mol. Sci.* **2021**, *22* (14), 7347.
(27) Cysewski, P.; Przybyłek, M.; Kowalska, A.; Tymorek, N. Thermodynamics and Intermolecular Interactions of Nicotinamide in Neat and Binary Solutions: Experimental Measurements and COSMO-RS Concentration Dependent Reactions Investigations. *Int. J. Mol. Sci.* **2021**, *22* (14), 7365.
(28) Mahmoudabadi, S. Z.; Pazuki, G. Investigation of COSMO-SAC Model for Solubility and Cocrystal Formation of Pharmaceutical Compounds. *Sci. Rep.* **2020**, *10* (1), 19879.
(29) Mullins, P. E. *Application of COSMO-SAC to Solid Solubility in Pure and Mixed Solvent Mixtures for Organic Pharmacological Compounds*, 2007.
(30) Wu, H.; Wang, J.; Zhou, Y.; Guo, N.; Liu, Q.; Zong, S.; Bao, Y.; Hao, H. Solid-Liquid Phase Equilibrium and Dissolution Properties of Ethyl Vanillin in Pure Solvents. *J. Chem. Thermodyn.* **2017**, *105*, 345−351.
(31) Havkin-Frenkel, D. Vanillin. *Kirk-Othmer Encyclopedia of Chemical Technology*; Wiley, 2018; pp 1−12.
(32) Hussain, K.; Thorsen, G.; Malthe-Sørenssen, D. Nucleation and Metastability in Crystallization of Vanillin and Ethyl Vanillin. *Chem. Eng. Sci.* **2001**, *56* (7), 2295−2304.
(33) Blaikie, L.; Kay, G.; Kong Thoo Lin, P. Synthesis and in Vitro Evaluation of Vanillin Derivatives as Multi-Target Therapeutics for the Treatment of Alzheimer's Disease. *Bioorg. Med. Chem. Lett.* **2020**, *30* (21), 127505.
(34) Cheng, H. M.; Chen, F. Y.; Li, C. C.; Lo, H. Y.; Liao, Y. F.; Ho, T. Y.; Hsiang, C. Y. Oral Administration of Vanillin Improves Imiquimod-Induced Psoriatic Skin Inflammation in Mice. *J. Agric. Food Chem.* **2017**, *65* (47), 10233−10242.
(35) Du, Y.; Wang, H.; Du, S.; Wang, Y.; Huang, C.; Qin, Y.; Gong, J. The Liquid-Liquid Phase Separation and Crystallization of Vanillin in 1-Propanol/Water Solution. *Fluid Phase Equilib.* **2016**, *409*, 84−91.
(36) Shakeel, F.; Haq, N.; Siddiqui, N. A. Solubility and Thermodynamic Function of Vanillin in Ten Different Environmentally Benign Solvents. *Food Chem.* **2015**, *180*, 244−248.
(37) Guo, N.; Hou, B.; Wu, H.; Huang, J.; Tao, X.; Huang, X.; Yin, Q.; Hao, H. Determination and Correlation of Ethyl Vanillin Solubility in Different Binary Solvents at Temperatures from 273.15 to 313.15 K. *J. Chem. Eng. Data* **2017**, *62* (6), 1788−1796.
(38) Yang, J.; Xu, S.; Wang, J.; Gong, J. Nucleation Behavior of Ethyl Vanillin: Balance between Chemical Potential Difference and Saturation Temperature. *J. Mol. Liq.* **2020**, *303*, 112609.
(39) Akay, S.; Kayan, B.; Jouyban, A.; Martínez, F.; Acree, W. E. Equilibrium Solubility of Vanillin in Some (Ethanol + Water) Mixtures: Determination, Correlation, Thermodynamics and Preferential Solvation. *J. Mol. Liq.* **2021**, *342*, 117529.
(40) Hamedi, M. H.; Laurent, B.; Grolier, J. P. E. Construction of Solid-Liquid Phase Diagrams in Ternary Systems by Titration Calorimetry. *Thermochim. Acta* **2006**, *445* (1), 70−74.
(41) Svärd, M.; Gracin, S.; Rasmuson, Å. C. Oiling out or Molten Hydrate—Liquid-Liquid Phase Separation in the System Vanillin-Water. *J. Pharm. Sci.* **2007**, *96* (9), 2390−2398.
(42) De Albuquerque, I.; Mazzotti, M. Crystallization Process Design Using Thermodynamics to Avoid Oiling out in a Mixture of Vanillin and Water. *Cryst. Growth Des.* **2014**, *14* (11), 5617−5625.
(43) Prausnitz, J. M.; Lichtenthaler, R. N.; de Azevedo, E. G. *Molecular Thermodynamics of Fluid-Phase Equilibria*, 3rd ed.; Prentice Hall PTR: NJ, 1999.
(44) Temprado, M.; Roux, M. V.; Chickos, J. S. Some Thermophysical Properties of Several Solid Aldehydes. *J. Therm. Anal. Calorim.* **2008**, *94* (1), 257−262.
(45) Dassault Systèmes. BIOVIA COSMOtherm. 2021. http://www.3ds.com (accessed Jan 23, 2024).
(46) *TURBOMOLE V7.4. A Development of University of Karlsruhe and Forschungszentrum Karlsruhe GmbH, 1989−2007, TURBOMOLE GmbH, Since 2007*, 2019, available from https://www.turbomole.org/.
(47) Klamt, A. *COSMO-RS: From Quantum Chemistry to Fluid Phase Thermodynamics and Drug Design*; Elsevier Science, 2005.
(48) Frisch, M. J.; Trucks, G. W.; Schlegel, H. B.; Scuseria, G. E.; Robb, M. A.; Cheeseman, J. R.; Scalmani, G.; Barone, V.; Mennucci, B.; Petersson, G. A.; Nakatsuji, H.; Caricato, M.; Li, X.; Hratchian, H. P.; Izmaylov, A. F.; Bloino, J.; Zheng, G.; Sonnenberg, J. L.; Hada, M.; Ehara, M.; Toyota, K.; Fukuda, R.; Hasegawa, J.; Ishida, M.; Nakajima, T.; Honda, Y.; Kitao, O.; Nakai, H.; Vreven, T.; Montgomery, J. A.; Peralta, J. E.; Ogliaro, F.; Bearpark, M.; Heyd, J. J.; Brothers, E.; Kudin, K. N.; Staroverov, V. N.; Kobayashi, R.; Normand, J.; Raghavachari, K.; Rendell, A.; Burant, J. C.; Iyengar, S. S.; Tomasi, J.; Cossi, M.; Rega, N.; Millam, J. M.; Klene, M.; Knox, J. E.; Cross, J. B.; Bakken, V.; Adamo, C.; Jaramillo, J.; Gomperts, R.; Stratmann, R. E.; Yazyev, O.; Austin, A. J.; Cammi, R.; Pomelli, C.; Ochterski, J. W.; Martin, R. L.; Morokuma, K.; Zakrzewski, V. G.; Voth, G. A.; Salvador, P.; Dannenberg, J. J.; Dapprich, S.; Daniels, A. D.; Farkas, Ö.; Foresman, J. B.; Ortiz, J. V.; Cioslowski, J.; Fox, D. J. *Gaussian 09*, Revision A.02, 2009.
(49) NIST Computational Chemistry Comparison and Benchmark Database. https://cccbdb.nist.gov/vibscalejustx.asp (accessed Dec 15, 2023).
(50) Balachandran, V.; Parimala, K. Vanillin and Isovanillin: Comparative Vibrational Spectroscopic Studies, Conformational Stability and NLO Properties by Density Functional Theory Calculations. *Spectrochim. Acta, Part A* **2012**, *95*, 354−368.
(51) Araújo, C. F.; Ribeiro-Claro, P.; Vaz, P. D.; Rudić, S.; Serrano, R. A. F.; Silva, L. P.; Coutinho, J. A. P.; Nolasco, M. M. Exploring Asymmetry Induced Entropy in Tetraalkylammonium-Urea DES Systems: What Can Be Learned from Inelastic Neutron Scattering? *Phys. Chem. Chem. Phys.* **2024**, *26*, 5969−5977.
(52) Nolasco, M. M.; Rodrigues, L. C.; Araújo, C. F.; Coimbra, M. M.; Ribeiro-Claro, P.; Vaz, P. D.; Rudić, S.; Silvestre, A. J. D.; Bouyahya, C.; Majdoub, M.; Sousa, A. F. From PEF to PBF: What Difference Does the Longer Alkyl Chain Make a Computational Spectroscopy Study of Poly(Butylene 2,5-Furandicarboxylate). *Front. Chem.* **2022**, *10*, 1056286.
(53) Nolasco, M. M.; Parker, S. F.; Vaz, P. D.; Ribeiro-Claro, P. J. A. Intermolecular Interactions in 3-Aminopropyltrimethoxysilane, N-Methyl-3-Aminopropyltrimethoxysilane and 3-Aminopropyltriethoxysilane: Insights from Computational Spectroscopy. *Int. J. Mol. Sci.* **2023**, *24* (23), 16634.
(54) Vanillin Infrared Spectrum. https://webbook.nist.gov/cgi/cbook.cgi?ID=C121335&Type=IR-SPEC&Index=0#IR-SPEC (accessed Nov 30, 2023).
(55) Nicolaou, M.; Senn, H.; Gibson, E.; Vilà-Nadal, L. IR of Vanillin: A Classic Study with a Twist. *ChemRxiv* **2023**.
(56) Nieger, M. *CCDC 659428: Experimental Crystal Structure Determination*, 2008.
(57) Cesari, L.; Namysl, S.; Canabady-Rochelle, L.; Mutelet, F. Phase Equilibria of Phenolic Compounds in Water or Ethanol. *Fluid Phase Equilib.* **2017**, *453*, 58−66.
(58) Paduszyński, K.; Królikowska, M. Extensive Evaluation of Performance of the COSMO-RS Approach in Capturing Liquid−Liquid Equilibria of Binary Mixtures of Ionic Liquids with Molecular Compounds. *Ind. Eng. Chem. Res.* **2020**, *59* (25), 11851−11863.

https://doi.org/10.1021/acs.iecr.4c00652
Ind. Eng. Chem. Res. 2024, 63, 9565−9575